Available online at www.sciencedirect.com
ScienceDirect
Journal of Sound and Vibration 320 (2009) 322–338
JOURNAL OF SOUND AND VIBRATION
www.elsevier.com/locate/jsvi

Vibration and acoustic response of a composite plate with inherent material damping in a thermal environment

P. Jeyaraj, N. Ganesan, Chandramouli Padmanabhan*

Machine Design Section, Department of Mechanical Engineering, Indian Institute of Technology Madras, Chennai 600 036, India

Received 29 May 2008; received in revised form 25 July 2008; accepted 2 August 2008
Handling Editor: L.G. Tham
Available online 20 September 2008

Abstract

This paper presents numerical studies on the vibration and acoustic response characteristics of a fiber-reinforced composite plate in a thermal environment by considering the inherent material damping property of the composite material. Initially the critical buckling temperature is obtained, followed by free and forced vibration analyses considering the pre-stress due to the imposed thermal environment. The vibration response predicted is then used to compute the sound radiation. The critical buckling temperature and vibration response are obtained using the finite element method based on the Classical Laminate Plate Theory (CLPT) while sound radiation characteristics are obtained using a coupled FEM/BEM technique. It is found that the vibration response of the structure reduces with an increase in uniform temperature rise for both Glass Epoxy and PEEK/IM7 materials, but the overall sound radiation of the plate reduces only marginally due to interaction between reduced stiffness and enhanced damping.

1. Introduction

Damping is an important factor in the dynamic design of any engineering component as it influences the vibration and noise levels significantly. It also controls the fatigue life and impact resistance of the structures. Fiber-reinforced composite structures are extensively used in aerospace, automobile, ship-building industries and other engineering applications due to their high ratio of strength and stiffness to weight. Fiber-reinforced composite materials have inherent material damping because of fiber–matrix interaction which is usually more than that of the conventional isotropic materials.

Structures can be exposed to moisture and heat during their service life. Thus, knowledge of the dynamic behavior of a structure over a range of temperatures is essential for the design of structures in a thermal environment. Thermal stresses due to aerodynamic heating may induce buckling and dynamic instability in structures.The pre-stress effect due to thermal load will affect the dynamic behavior of the structure due to the change in the stiffness of the structure.

*Corresponding author. Tel.: +91 44 2257 4690.
E-mail address: mouli@iitm.ac.in (C. Padmanabhan).

0022-460X/$ - see front matter © 2008 Elsevier Ltd. All rights reserved.
doi:10.1016/j.jsv.2008.08.013

Initial investigations on the damping analysis of fiber-reinforced composite materials have been reviewed extensively by Chandra et al. [1]. Rikards [2] used a modal strain energy-based finite element method to obtain the loss factors of a laminated composite plate. Melo and Radford [3] analyzed the time and temperature dependence of the viscoelastic properties of Carbon Fiber Reinforced Plastic (CFRP) material experimentally. They found that there is a significant change in the loss factor compared to the elastic modulus due to a change in temperature.

The buckling behavior of fiber-reinforced composite plates subjected to a thermal load has been analyzed extensively with the help of both analytical [4] and finite element methods [5,6]. The pre-stress effect due to thermal load will affect the free vibration behavior of the structure and the natural frequencies of the structure decreases with an increase in thermal load. The modal loss factor increases with the temperature; when the uniform temperature rise approaches the critical buckling temperature there is a significant increase in the modal loss factor [7].

Temperature and moisture variations lead to a thermo-elastic-dynamic response in a structure as well as noise radiation from such structures [8]. Park et al. [9] investigated the effects of support properties on the sound radiated from the plate and found that both the velocity response and the sound radiation are strongly influenced by dissipation of vibration energy at the edges. Qiao and Huang [10] analyzed six different boundary conditions to investigate the influence of boundary conditions on the sound radiation of a plate under a harmonically excited point force. They found that boundary conditions have a large effect on the sound radiated from rectangular plates. The aim of the present work is to analyze the vibration and acoustic response characteristics of a composite plate under a thermal environment subjected to mechanical time-varying harmonic excitations by considering the inherent material damping associated with the composite materials.

2. Formulation

The Finite Element Method (FEM) is used to predict the critical buckling temperature, natural frequencies, loss factors and vibration response of the plate. A two-dimensional four-noded quadrilateral thin-plate element having five degrees of freedom per node formulated based on the Classical Laminate Plate Theory (CLPT) is used in the present work, which leads to the following displacement field; more details of the formulation can be found in [11].

$$\begin{Bmatrix} u \\ v \\ w \end{Bmatrix} = \begin{Bmatrix} u_\circ + z\dfrac{\partial w}{\partial x} \\ v_\circ + z\dfrac{\partial w}{\partial y} \\ w_\circ \end{Bmatrix} \tag{1}$$

where u, v and w are the components of the displacement along x, y and z directions with x and y on the plane of the plate and z along the thickness direction. The subscript $\circ$ refers to the reference plane. The strain displacement relations are given by

$$\begin{Bmatrix} \varepsilon_x \\ \varepsilon_y \\ \gamma_{xy} \end{Bmatrix} = \begin{Bmatrix} \dfrac{\partial u_\circ}{\partial x} \\ \dfrac{\partial v_\circ}{\partial y} \\ \dfrac{\partial u_\circ}{\partial y} + \dfrac{\partial v_\circ}{\partial x} \end{Bmatrix} - \begin{Bmatrix} z\dfrac{\partial^2 w_\circ}{\partial x^2} \\ z\dfrac{\partial^2 w_\circ}{\partial y^2} \\ 2z\dfrac{\partial^2 w_\circ}{\partial x \partial y} \end{Bmatrix} \tag{2}$$

$$\begin{Bmatrix} \varepsilon_x \\ \varepsilon_y \\ \gamma_{xy} \end{Bmatrix} = \begin{Bmatrix} \varepsilon_x^\circ \\ \varepsilon_y^\circ \\ \gamma_{xy}^\circ \end{Bmatrix} + z\begin{Bmatrix} \kappa_x \\ \kappa_y \\ \kappa_{xy} \end{Bmatrix}, \quad \{\varepsilon\} = \{\varepsilon^\circ\} + z\{\kappa\} \tag{3}$$

where ε° and κ are the strain and the curvature of the reference plane. The constitutive relations for a laminated plate accounting for thermal effects can be written as [11]

$$\begin{pmatrix} \sigma_x \\ \sigma_y \\ \sigma_{xy} \end{pmatrix} = \begin{pmatrix} \overline{Q}_{11} & \overline{Q}_{12} & \overline{Q}_{16} \\ \overline{Q}_{12} & \overline{Q}_{22} & \overline{Q}_{26} \\ \overline{Q}_{16} & \overline{Q}_{26} & \overline{Q}_{66} \end{pmatrix} \begin{pmatrix} \varepsilon_x - \alpha_x \Delta T \\ \varepsilon_y - \alpha_y \Delta T \\ \varepsilon_{xy} - \alpha_{xy} \Delta T \end{pmatrix} \tag{4}$$

where $\overline{Q}_{ij}$ is the transformed reduced stiffness, α_x, α_y and α_{xy} are the coefficients of thermal expansion along x, y and shear directions and ΔT is the temperature difference (assumed to be uniform). The stress resultants and stress couples are given by

$$\begin{Bmatrix} N_x \\ N_y \\ N_{xy} \end{Bmatrix} = \int_{-h/2}^{h/2} \begin{Bmatrix} \sigma_x \\ \sigma_y \\ \sigma_{xy} \end{Bmatrix} \mathrm{d}z, \quad \begin{Bmatrix} M_x \\ M_y \\ M_{xy} \end{Bmatrix} = \int_{-h/2}^{h/2} \begin{Bmatrix} \sigma_x \\ \sigma_y \\ \sigma_{xy} \end{Bmatrix} z \, \mathrm{d}z \tag{5}$$

The total potential energy Π of the plates is $\Pi = U_b + V$, where U_b is the strain energy of bending and V is the potential energy due to external loads. A four-noded quadrilateral plate element with five degrees-of-freedom (dof) is used for the finite element solution of the laminates. The shape function of the displacement field is defined as

$$[\, u \, v \, w \, \theta_x \, \theta_y \,]^{\mathrm{T}} = [N]\{\delta\} \tag{6}$$

where $[N]$ and $\{\delta\}$ are the shape function matrix and the nodal variable vector, respectively. The structure stiffness and mass matrices of the plate are obtained by using the minimum potential energy principle. The structure stiffness matrix $[K]$ can be written as

$$[\, K \,] = \int \int \, [B]^{\mathrm{T}} [D^*] [B] \, \mathrm{d}x \, \mathrm{d}y, \quad [\, D^* \,] = \begin{bmatrix} A_{ij} & B_{ij} \\ B_{ij} & D_{ij} \end{bmatrix} \tag{7}$$

where A_{ij}, B_{ij} and D_{ij} are the coefficients of extensional, bending–extensional coupling and bending stiffness matrices. These are obtained as

$$(A_{ij}, B_{ij}, D_{ij}) = \int_{-h/2}^{h/2} \overline{Q}_{ij} (1, z, z^2) \mathrm{d}z, \quad (i, j = 1, 2, 6) \tag{8}$$

Since all the elastic moduli associated with the composite materials considered in the present analysis are complex, the structural stiffness matrix $[K]$ is complex and can be decomposed as

$$[K] = [K_R] + j[K_I] \tag{9}$$

where $[K_R]$ and $[K_I]$ are the real and imaginary parts of the structure stiffness matrix, respectively. The mass matrix of the plate can be written as

$$[M] = \int_{-h/2}^{h/2} \int_{-h/2}^{h/2} [N]^{\mathrm{T}} \, [P] \, [N] \, \mathrm{d}x \, \mathrm{d}y \tag{10}$$

where $[P]$ is the mass property matrix. The geometric stiffness matrix $[K_\sigma]$ is obtained from the work done by the membrane forces developed due to thermal load. The membrane forces S_x, S_y and S_{xy} are specified in terms of membrane stresses σ_x, σ_y and shear stress τ_{xy} developed due to thermal load and are calculated from a static analysis. The nonlinear membrane strains associated with lateral deflection (ω) of the plate can be

written as

$$\begin{Bmatrix} \varepsilon_x \\ \varepsilon_y \\ \gamma_{xy} \end{Bmatrix} = \begin{Bmatrix} \frac{1}{2}\left(\frac{\partial\omega}{\partial x}\right)^2 \\ \frac{1}{2}\left(\frac{\partial\omega}{\partial y}\right)^2 \\ \left(\frac{\partial\omega}{\partial x}\right)\left(\frac{\partial\omega}{\partial y}\right) \end{Bmatrix} \tag{11}$$

The change in membrane strain energy associated with constant membrane forces and the nonlinear membrane strains can be written as

$$U_m = \int \left[\frac{1}{2}S_x\left(\frac{\partial\omega}{\partial x}\right)^2 + \frac{1}{2}S_y\left(\frac{\partial\omega}{\partial y}\right)^2 + S_{xy}\left(\frac{\partial\omega}{\partial x}\right)\left(\frac{\partial\omega}{\partial y}\right)\right] \mathrm{d}A \tag{12}$$

$$U_m = \frac{1}{2}\int\int \begin{Bmatrix} \frac{\partial\omega}{\partial x} \\ \frac{\partial\omega}{\partial y} \end{Bmatrix}^{\mathrm{T}} \begin{bmatrix} S_x & S_{xy} \\ S_{xy} & S_y \end{bmatrix} \begin{Bmatrix} \frac{\partial\omega}{\partial x} \\ \frac{\partial\omega}{\partial y} \end{Bmatrix} \mathrm{d}x\,\mathrm{d}y \tag{13}$$

Now the displacement vector is given by

$$\{q\} = \sum_{i=1}^{4} [N_i]\{q_i\}^e \tag{14}$$

The derivatives are:

$$\begin{Bmatrix} \frac{\partial\omega}{\partial x} \\ \frac{\partial\omega}{\partial y} \end{Bmatrix} = [B_g]\{q\} \tag{15}$$

This, when substituted into Eq. (13), leads to

$$U_m = \frac{1}{2}\{q\}^{\mathrm{T}}[K_\sigma]\{q\}, \quad [K_\sigma] = \int\int [B_g]^{\mathrm{T}} \begin{bmatrix} S_x & S_{xy} \\ S_{xy} & S_y \end{bmatrix} [B_g]\,\mathrm{d}x\,\mathrm{d}y \tag{16}$$

3. Analysis approach

FEM is used to find the critical buckling temperature, the effects of thermal load on the natural frequencies and the vibration response of the plate. The thermal load is assumed to be created in the plate due to a uniform temperature distribution across the surface of the plate. The thermal load applied on the structure will induce membrane forces, which in turn influence the lateral deflections associated with the plate. The resistance to bending deformation is reduced when membrane forces are compressive. These pre-loads on the plate due to the thermal environment are calculated using a static analysis. The pre-stressed modal and harmonic analyses are carried out with critical buckling temperature as a parameter to analyze the effect of thermal load on the natural frequencies and vibration response. The entire analysis approach is summarized in Fig. 1. When the temperature of the plate is increased from the ambient by ΔT, thermal stresses develop in the plate (for any boundary condition with at least one edge restrained). This stress state (static) is used to calculate the geometric stiffness matrix $[K_\sigma]$. Following this a buckling analysis is carried out using the structural and geometric stiffness matrices $[K]$ and $[K_\sigma]$

$$([K] + \lambda_i[K_\sigma])\{\psi_i\} = 0 \tag{17}$$

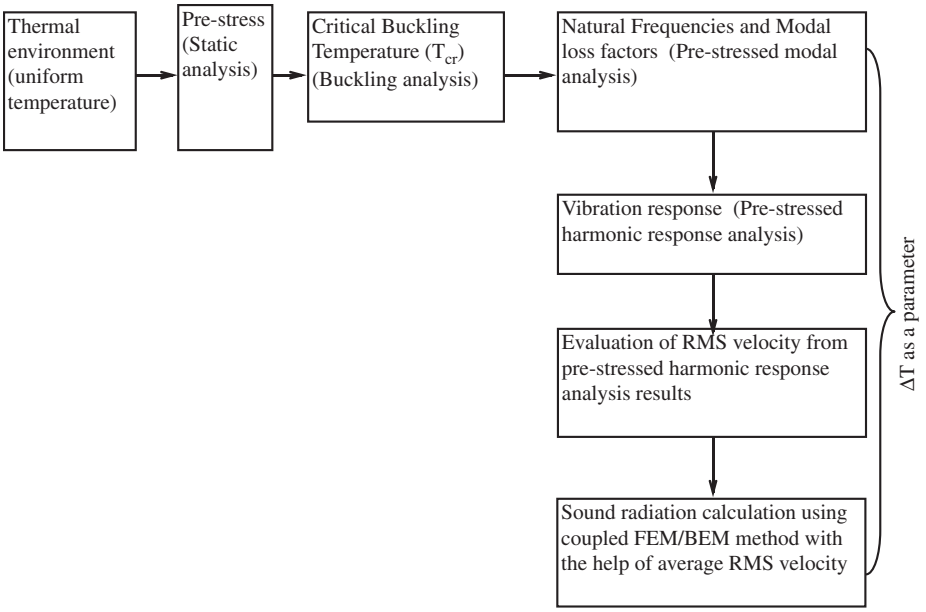

Fig. 1. A flowchart of the analysis approach.

where λ_i is the ith eigen value and ψ_i is the corresponding eigen vector. The product of the lowest eigenvalue λ_1 and the temperature rise ΔT yields the critical buckling temperature, T_{cr}, that is $T_{\mathrm{cr}} = \lambda_1 \Delta T$. Physically, T_{cr} defines the temperature at which the plate buckles due to thermal stresses. Since the structure is pre-loaded due to the thermal field, the natural frequencies of the structure are modified as these loads produce stresses which change the structural stiffness. Pre-stressed modal analysis is carried out to find the natural frequency of the pre-loaded structure. The natural frequency at any given temperature can be calculated by evaluating the geometric stiffness matrix at that temperature and by solving the eigenvalue problem as given below:

$$(([K_R] + [K_\sigma]) - \omega_k^2[M])\{\phi_k\} = 0 \tag{18}$$

where $[M]$ is the structural mass matrix, while ω_k is the circular natural frequency of the pre-stressed structure and ϕ_k the corresponding mode shape. Similarly, the kth modal loss factor (η_k) at any given temperature can be obtained from the following equation:

$$\eta_k = \frac{\{\phi_k\}^{\mathrm{T}}[K_I]\{\phi_k\}}{\{\phi_k\}^{\mathrm{T}}[K_R + K_\sigma]\{\phi_k\}} \tag{19}$$

After the computation of the natural frequencies, loss factors and mode shapes a pre-stressed harmonic analysis is carried out to determine the vibration response of the pre-loaded structure. The general equation of motion for a pre-stressed structure is

$$[M]\{\ddot{U}\} + [C]\{\dot{U}\} + ([K] + [K_\sigma])\{U\} = \{F(t)\} \tag{20}$$

where $F(t)$ is the applied load vector (assumed to be time-harmonic) and $\ddot{U}$, $\dot{U}$ and U are the acceleration, velocity and displacement vector of the plate. Using a set of modal coordinates y_k, $k = 1, 2, \ldots, n$, where n is the total number of degrees of freedom. The transformation from physical coordinates to modal coordinates can be written as

$$\{U\} = \sum_{k=1}^{n} \{\overline{\phi}_k\} y_k = [\overline{\phi}]\{y\} \tag{21}$$

where $[\overline{\phi}]$ is the modal matrix. Eq. (20) can then be written as

$$[M][\overline{\phi}]\{\ddot{y}\} + [C][\overline{\phi}]\{\dot{y}\} + ([K_R] + [K_\sigma])[\overline{\phi}]\{y\} = \{F(t)\} \tag{22}$$

Pre-multiplying the above equation by $[\overline{\phi}]^{\mathrm{T}}$ and using the orthogonality relations after applying the orthogonal and normal conditions Eq. (22) becomes

$$\ddot{y}_k + 2\omega_k\xi_k\dot{y}_k + \omega_i^2 y_k = F_k, \quad k = 1, 2, \ldots, m \tag{23}$$

where $F_k = [\overline{\phi}]^{\mathrm{T}}\{F(t)\}$. Since $\xi_k = \eta_k/2$ the above equation becomes

$$\ddot{y}_k + \omega_k\eta_k\dot{y}_k + \omega_i^2 y_k = F_k \tag{24}$$

The vibration response is obtained by solving the above uncoupled equation.

In the Boundary Element Method, the boundary is divided into N elements and the Helmholtz equation is discretized for a given node i so that the discrete form of the integral equation can be written as

$$cp_i - \sum_{j=1}^{N}\int_{S_j} p\frac{\partial g}{\partial \widehat{n}}\,\mathrm{d}S = -\sum_{j=1}^{N}\int_{S_j} g\frac{\partial p}{\partial \widehat{n}}\,\mathrm{d}S \tag{25}$$

where c is a coefficient which is either 1, 0 or $\frac{1}{2}$ depending on whether the field point is in the volume, outside the volume or on the smooth boundary, p is the acoustic pressure, S_j is the surface of the element j on the boundary, g is the free space Green's function in the frequency domain and $\widehat{n}$ is the surface unit normal vector. As the normal velocity on the surface $v = (i/\rho_o\omega)\partial p/\partial\widehat{n}$ Eq. (25) becomes

$$cp_i - \sum_{j=1}^{N}\int_{S_j} p\overline{g}\,\mathrm{d}S = -\mathrm{i}\rho_o\omega\sum_{j=1}^{N}\int_{S_j} gv\,\mathrm{d}S \tag{26}$$

where $\overline{g} = \partial g/\partial\widehat{n}$. For a node on the constant element (p and v are constant over each element) Eq. 26 can be written as

$$\frac{1}{2}p_i - \sum_{j=1}^{N}\int_{S_j}(\overline{g}\,\mathrm{d}S)p_j = -i\rho_o\omega\sum_{j=1}^{N}\int_{S_j}(g\,\mathrm{d}S)v_j \tag{27}$$

If one defines the influence coefficients $\overline{H}_{ij} = \int_{S_j}\overline{g}\,\mathrm{d}S$; $G_{ij} = \int_{S_j} g\,\mathrm{d}S$, which are integrals relating node i, where the fundamental solution is acting, to any other node j. For a particular node i Eq. (27) takes the form

$$\frac{1}{2}p_i - \sum_{j=1}^{N}\overline{H}_{ij}p_j = -i\rho_o\omega\sum_{j=1}^{N}G_{ij}v_j \tag{28}$$

by introducing $H_{ij} = \frac{1}{2}\delta_{ij} - \overline{H}_{ij}$ where δ_{ij} is Knonecker's delta. Eq. (28) can now be written as

$$\sum_{j=1}^{N}\overline{H}_{ij}p_j = i\rho_o\omega\sum_{j=1}^{N}G_{ij}v_j \tag{29}$$

If Eq. (29) is repeated for every node point i, a system of equations obtained can be expressed in matrix form as

$$[H]\{p\} = i\rho_o\omega[G]\{v\} \tag{30}$$

where $[H]$ and $[G]$ are the boundary integral influence matrices, $\{p\}$ and $\{v\}$ are the acoustic pressure and the normal velocity of the boundary element nodes of the fluids, respectively, at the fluid–structure interface and ρ_o is the density of the fluid. The reader is referred to Ref. [12] for detailed information on the formulation of direct BEM/FEM.

4. Validation studies

4.1. Validation for critical buckling temperature evaluation

A single-layer thin (side/thickness = 40) Kevlar/Epoxy square plate with fiber orientation angle 45° and having all edges clamped analyzed by Huang and Tauchert [4] is considered for the validation of the critical buckling temperature. Huang and Tauchert [4] used an analytical method to predict the critical buckling

temperature while the present method uses a four-noded quadrilateral element formulated based on the Classical Laminate Plate Theory (CLPT). The material properties of Kevlar/Epoxy analyzed are as follows [4]: $E_1 = 76\,\text{GPa}$; $E_2 = 5.5\,\text{GPa}$; $G_{12} = G_{13} = 2.3\,\text{GPa}$; $G_{23} = 1.5\,\text{GPa}$; $v_{12} = 0.34$; $\alpha_1 = -4 \times 10^{-6}/^{\circ}\text{C}$; and $\alpha_2 = 79 \times 10^{-6}/^{\circ}\text{C}$ where E_1 and E_2 are Young's modulus of the lamina along major (fiber direction) and minor axes, respectively, G_{12}, G_{13} and G_{23} are shear moduli of the lamina, while v_{12} is the major Poisson's ratio. The coefficients of thermal expansion along major and minor axes are α_1 and α_2, respectively. The critical buckling temperature evaluated using the present approach is 131 °C which matches very well with the value reported by Huang and Tauchert [4] which is 132 °C.

4.2. Validation for natural frequencies and loss factors

A simply supported, four-ply laminated carbon fiber reinforced plastic (CFRP) square plate with fibers oriented at an angle 45° analyzed by Alam and Asnani [13] is considered for the validation of frequency and loss factor. The ratio of the length to the thickness of the plate considered is 150. The material properties of the CFRP considered are $E_1 = 211\,\text{GPa}$; $E_2 = 5.3(1 + 0.5j)\,\text{GPa}$; $G_{12} = G_{13} = 2.6(1 + 0.5j)\,\text{GPa}$; $G_{23} = 1.3(1 + 0.5j)\,\text{GPa}$; $v_{12} = 0.25$; and density $\rho = 1524\,\text{kg/m}^3$. Alam and Asnani [13] used a variational principle to obtain the resonant frequency parameter and loss factors while FEM is used here. Table 1 shows the comparison of the resonant frequency parameter λ_r for the flexural mode I and the extensional modes II and III and the associated system loss factor η. The expression for resonant frequency parameter is $\lambda_r = \rho t^2 \omega^2 / E_1$ where ρ is the mass density of the material considered, t is the thickness of the plate and ω is the resonant frequency in radians per second. From Table 1 it is clear that both the natural frequencies and the modal loss factors obtained in the present work agree very well with the results reported by Alam and Asnani [13].

4.3. Validation of sound radiation calculation

A simply supported isotropic rectangular plate with dimensions $0.455\,\text{m} \times 0.379\,\text{m} \times 0.003\,\text{m}$ analyzed by Li and Li [14] is considered for the validation of sound power-level calculation using SYSNOISE. The plate is made of steel with Young's modulus $E = 210\,\text{GPa}$, density $\rho = 7850\,\text{kg/m}^3$ and Poisson's ratio $v = 0.3$. The plate is assumed to be vibrating in air whose density is $\rho_a = 1.21\,\text{kg/m}^3$ with a speed of sound $c = 343\,\text{m/s}$. A harmonic excitation of 1 N is applied at the center of the plate and a structural damping ratio of 0.01 for all modes is assumed for harmonic response analysis. Li and Li [14] used four-noded isoparametric elements for their structural finite element model and calculated sound power level using the Rayleigh integral. In the present work, the plate is modeled using 16×16 plate elements formulated based on the Classical Laminate Plate Theory. The computed natural frequencies are compared with those reported by Li and Li [14] in Table 2. The average rms velocity is calculated for each frequency from the pre-stressed harmonic analysis results. The sound power level of the plate is calculated using SYSNOISE by assuming that the entire plate is vibrating with an average rms velocity at each frequency. Fig. 2 show the comparison of sound power level obtained using average rms velocity (present) with the results reported by Li and Li [14]. The modes corresponding to modal indices (2,1), (2,2) and (1,2) will not be excited as the harmonic excitation force is at the center of the plate. Both the natural frequencies and the sound power levels match very well with those of Li and Li [14].

Table 1
Comparison of resonant frequency parameter and loss factor

Mode	Resonant frequency parameter λ_r		Loss factor (η)	
	Alam and Asnani [13]	Present work	Alam and Asnani [13]	Present work
I	0.204×10^8	0.203×10^8	0.0135	0.0132
II	0.688×10^6	0.682×10^6	0.499	0.496
III	0.284×10^4	0.281×10^4	0.0124	0.0121

Table 2
Comparison of natural frequencies (Hz) with Li and Li [14]

Modal indices	Li and Li [14]	Present work
(1, 1)	87	87
(2, 1)	193	193
(1, 2)	241	241
(2, 2)	345	346
(3, 1)	374	372

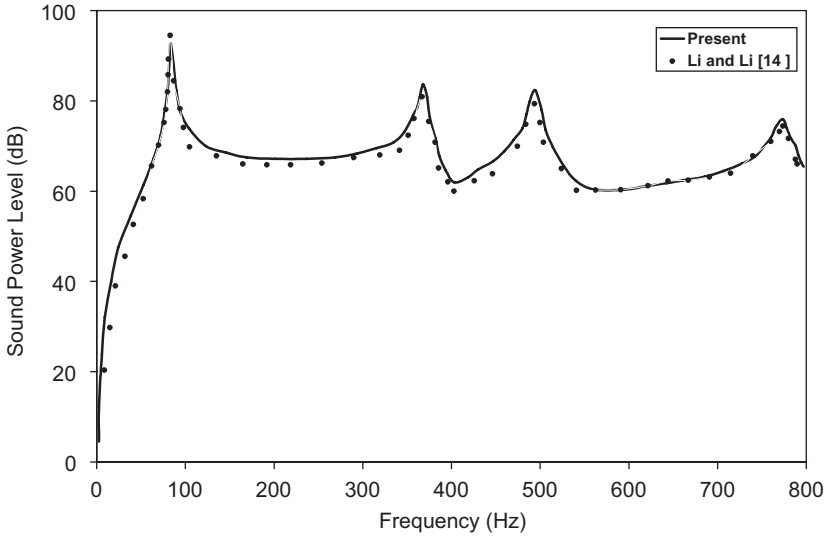

Fig. 2. Comparison of sound power level with Li and Li [14].

5. Results and discussion

A rectangular composite plate clamped at all its edges with dimensions $0.5\,\mathrm{m} \times 0.4\,\mathrm{m} \times 0.01\,\mathrm{m}$ is now considered for the detailed investigation. The plate is analyzed for two different fiber-reinforced composite materials namely Glass Epoxy and PEEK/IM7. The elastic material properties of the Glass/Epoxy are assumed to be temperature independent while the PEEK/IM7 properties are temperature dependent. The plate is assumed to have only one layer of fiber. The plate is assumed to be vibrating in air whose density is $\rho_a = 1.21\,\mathrm{kg/m^3}$ with a speed of sound $c = 343\,\mathrm{m/s}$. The material properties of the Glass Epoxy composite are $E_1 = 37.78(1 + 0.0014j)\,\mathrm{GPa}$; $E_2 = 10.9(1 + 0.0008j)\,\mathrm{GPa}$; $G_{12} = G_{13} = 4.91(1 + 0.011j)\,\mathrm{GPa}$; $v_{12} = 0.3$; $\rho = 1870\,\mathrm{kg/m^3}$; $\alpha_1 = 7 \times 10^{-6}/^{\circ}\mathrm{C}$; and $\alpha_2 = 2.3 \times 10^{-5}/^{\circ}\mathrm{C}$ and then temperature dependence of the viscoelastic properties of PEEK/IM7 composite materials is given in Table 3. The values of α_1 and α_2 of the PEEK/IM7 material are $-0.15 \times 10^{-6}/^{\circ}\mathrm{C}$ and $26.57 \times 10^{-6}/^{\circ}\mathrm{C}$, respectively. A convergence study has been carried out for the critical buckling temperature and natural frequencies without considering any thermal load for zero fiber orientation as given in Table 4. Based on the convergence study the plate is modeled using a 16×16 mesh.

5.1. Evaluation of critical buckling temperature T_{cr}

In the present work, the vibration and acoustic response of a fiber-reinforced composite plate for different fiber orientations has been analyzed by assuming that the structure is subjected to a uniform temperature rise above ambient temperature. The uniform temperature rise applied on the plate is varied from 0 to 100 °C for each fiber orientation and the corresponding variation in natural frequencies, loss factors, vibration and

Table 3
Temperature dependence of the viscoelastic properties of PEEK/IM7 [3]

Temperature (°C)	E_1 (GPa)	E_2 (GPa)	G_{12} (GPa)	ν_{12}	$\nu_{23}10^{-3}$	$\eta_1, 10^{-3}$	$\eta_2, 10^{-3}$	$\eta_6, 10^{-3}$
−20	155.4	10.2	7.4	0.34	0.48	4.7	7.8	8.8
0	155.1	10.1	7.3	0.34	0.49	4.5	7.5	10.5
20	154.9	10.0	7.2	0.34	0.49	5.1	7.2	10.6
40	154.7	10.0	7.1	0.34	0.49	5.2	7.7	11.5
60	154.5	9.9	7.1	0.35	0.49	5.7	8.5	13.5
80	154.3	9.8	7.0	0.35	0.5	6.8	9.3	14.6
100	154.0	9.7	7.0	0.35	0.5	7.2	10.1	14.8
120	153.8	9.6	6.9	0.35	0.5	7.0	12.1	14.9

Table 4
Convergence study for critical buckling temperature T_{cr} and natural frequencies

Critical buckling temperature T_{cr} (°C)	Mesh size				
	10 × 10	12 × 12	14 × 14	16 × 16	18 × 18
	132	131	131	131	131
Natural frequency (Hz)					
(1, 1)	266	264	264	264	264
(1, 2)	510	509	508	508	508
(2, 1)	568	567	567	566	566
(2, 2)	770	768	767	766	766
(1, 3)	912	908	906	905	905

Table 5
Critical buckling temperature for different fiber orientations for glass epoxy

Fiber orientation	Critical buckling temperature (°C)
0	133
15	129
30	123
45	127
60	144
75	174
90	186

acoustic response has been analyzed. The uniform temperature rise has been limited to 100 °C in order to keep the temperature below the glass transition temperature of the polymer material which is around 140 °C. To start with, the critical buckling temperature is obtained for different fiber orientations for Glass/Epoxy composite material and this is given in Table 5. In Table 5, it must be noted that the critical buckling temperature exceeds the glass transition temperature of the polymer matrix for the fiber orientations 60°, 75° and 90°. Thus, the plate is analyzed for different fiber orientations ranging from 0° to 45° in steps of 15°. Similarly, the critical buckling temperature of a PEEK/IM7 plate with a 0° fiber orientation is 307 °C for the dimensions 0.5 m × 0.4 m × 0.01 m, which also exceeds the glass transition temperature. Hence a plate with dimensions 0.5 m × 0.4 m × 0.005 m is considered to analyze the PEEK/IM7 composite material for which the critical buckling temperature obtained is 74 °C. The pre-stressed modal analysis is carried out for different values of fiber orientation by varying the uniform temperature rise applied on the plate from 0 °C to 100 °C, in order to determine the influence of the thermal environment on the natural frequencies and corresponding

Table 6
Variation of natural frequencies and loss factors with temperature

Fiber orientation rise (°C)	Uniform temperature (°C)	First mode	Second mode	Third mode	Fourth mode	Fifth mode
Glass/Epoxy						
0°	0	264(0.0049)	510(0.0073)	573(0.0028)	770(0.0053)	912(0.0078)
	30	234(0.0062)	471(0.0085)	543(0.0031)	732(0.0059)	871(0.0086)
	60	197(0.0088)	426(0.0102)	510(0.0035)	691(0.0066)	825(0.0096)
	90	151(0.0153)	377(0.0134)	475(0.0041)	648(0.0075)	777(0.0110)
	100	132(0.0262)	359(0.0163)	462(0.0047)	633(0.0081)	760(0.0124)
15°	0	265(0.0051)	514(0.0065)	568(0.0036)	768(0.0055)	938(0.0074)
	30	233(0.0064)	496(0.0075)	515(0.0039)	730(0.0061)	897(0.0081)
	60	195(0.0093)	432(0.0098)	498(0.0043)	688(0.0069)	851(0.0091)
	90	146(0.0168)	383(0.0126)	459(0.0051)	643(0.0079)	803(0.0101)
	100	126(0.0536)	365(0.0137)	445(0.0060)	628(0.0093)	786(0.0114)
30°	0	268(0.0051)	504(0.0051)	583(0.0051)	765(0.0058)	947(0.0036)
	30	235(0.0066)	467(0.0062)	544(0.0057)	727(0.0065)	908(0.0040)
	60	194(0.0098)	425(0.0076)	501(0.0067)	684(0.0073)	866(0.0045)
	90	141(0.0190)	379(0.0099)	453(0.0080)	638(0.0084)	822(0.0051)
	100	117(0.0215)	361(0.0105)	436(0.0093)	622(0.0094)	807(0.0061)
45°	0	279(0.0047)	478(0.0053)	643(0.0045)	753(0.0060)	889(0.0043)
	30	245(0.0061)	440(0.0063)	604(0.0051)	713(0.0067)	854(0.0048)
	60	204(0.0089)	397(0.0078)	561(0.0059)	669(0.0076)	804(0.0053)
	90	152(0.0163)	347(0.0102)	514(0.0071)	623(0.0085)	757(0.0059)
	100	130(0.0193)	329(0.0128)	497(0.0088)	606(0.0096)	740(0.0078)
PEEK/IM-7	0	241(0.0060)	343(0.0072)	542(0.0077)	614(0.0055)	683(0.0063)
	10	233(0.0062)	324(0.0078)	519(0.0081)	608(0.0059)	673(0.0065)
	30	214(0.0085)	278(0.0125)	453(0.0122)	601(0.0064)	647(0.0077)
	50	190(0.0132)	215(0.0232)	379(0.0191)	590(0.0078)	624(0.0100)
	70	129(0.0713)	157(0.0269)	293(0.0324)	573(0.0153)	585(0.0132)

modal loss factors and mode shapes. The results obtained from the pre-stressed modal analysis are given in Table 6. In Table 6, the values given in bracket represent modal loss factors associated with the corresponding modes. As the temperature rise is limited to 100 °C in the present study (i.e., the plate is not analyzed close to the critical buckling temperature due to glass transition temperature issues) the natural frequencies of the fundamental mode for different fiber orientations are not near zero. However, from the pre-stressed modal analysis carried out near the critical buckling temperature it is found that the fundamental mode frequency does go to zero and the loss factor increases to a very high value. This is due to a decrease in stiffness due to an increase in temperature. The mode shapes, however, are not significantly affected by thermal environment as seen in Fig. 3. For the PEEK/IM7 material, loss factors obtained by considering temperature-dependent and temperature-independent elastic properties are compared and it is found that there is no significant variation in loss factor.

5.2. Vibration and acoustic response studies

In order to compare the vibration response and sound radiation characteristics, a frequency range of 0−1500 Hz is chosen for different fiber orientations. Before carrying out the harmonic response analysis, an appropriate point of location of excitation of the harmonic force is chosen using the mode shapes of the plate for different fiber orientations. The location of excitation is chosen in such a way that it should not lie on the nodal lines of modes in the frequency range of 0−1500 Hz; this is done at room temperature but since the mode shapes are independent of temperature the excitations would still not coincide with any nodal lines. The pre-stressed harmonic analysis is carried out by applying a 1 N load at the location chosen for each

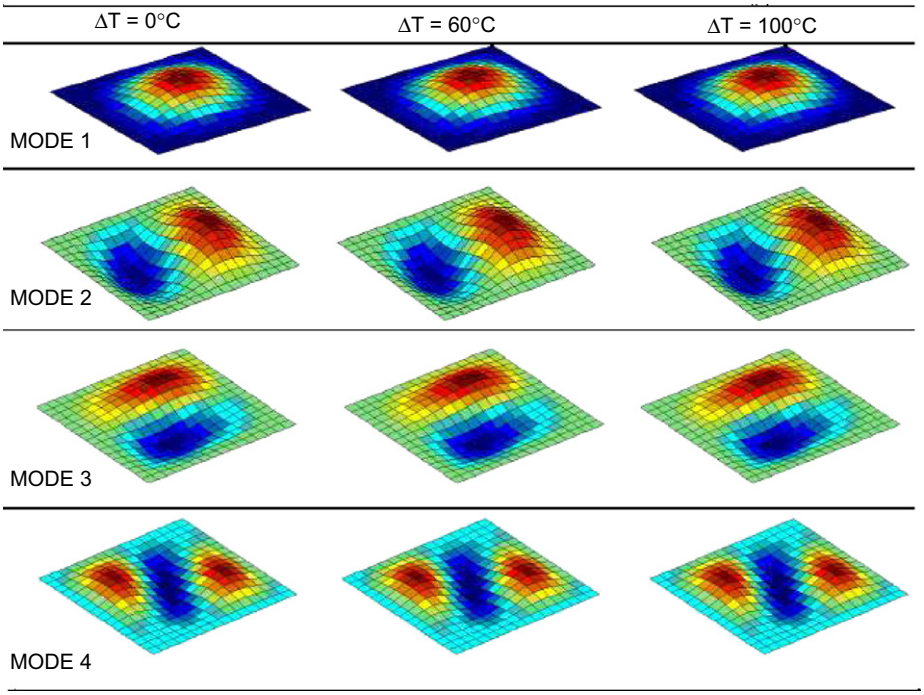

Fig. 3. Mode shapes at different values of uniform temperature rise.

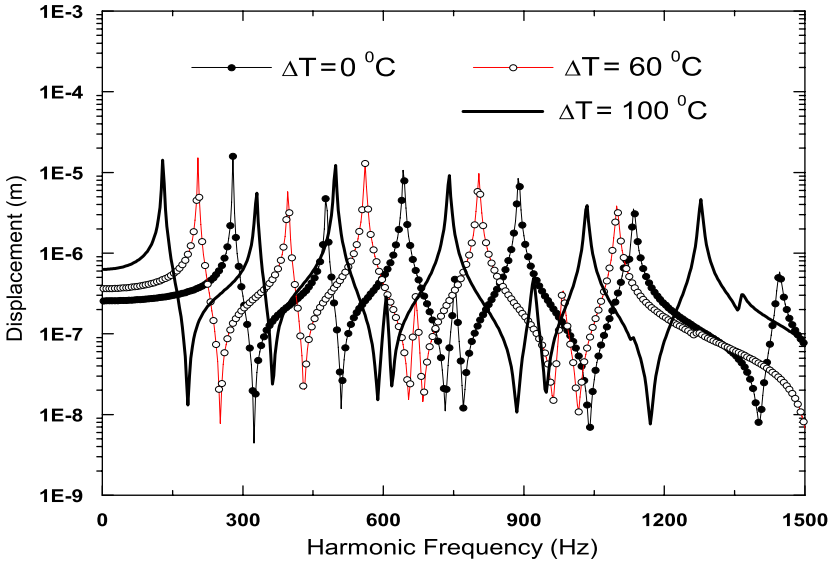

Fig. 4. Displacement at the point of excitation for a 45° fiber orientation of a Glass/Epoxy composite plate.

fiber orientation. The displacement and velocity response at the point of excitation are obtained for each fiber orientation. The average rms velocity of the plate has been calculated for each frequency and for each fiber orientation to give as an input for the sound radiation calculation. The direct boundary element method with the baffle option is used in SYSNOISE to obtain the acoustic characteristics. The sound power level and radiation efficiency for each fiber orientation is obtained.

Figs. 4–6 and 8 show the displacement response,velocity response, average rms velocity and sound power level, respectively, as the excitation frequency is varied for a 45° fiber orientation. Two trends can be seen: (i) the natural frequencies reduce with increasing temperature and (ii) the resonant amplitudes decrease

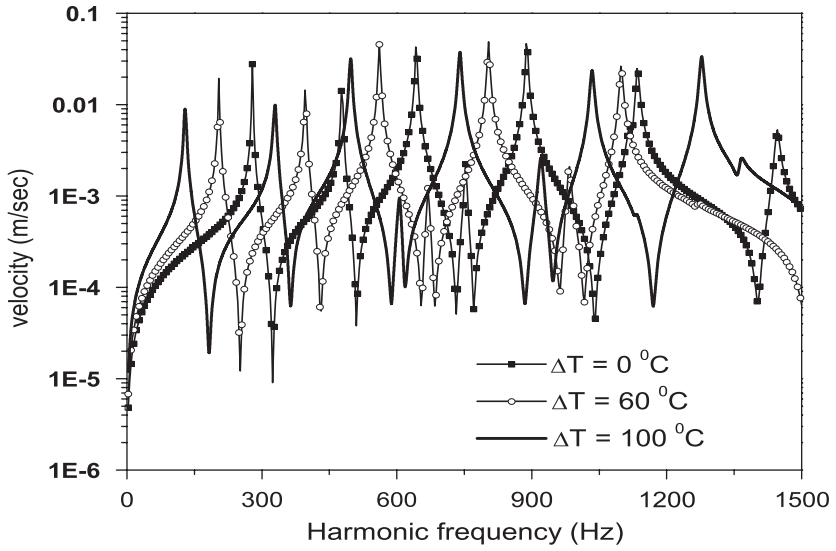

Fig. 5. Velocity at the point of excitation for a 45° fiber orientation of a Glass/Epoxy composite plate.

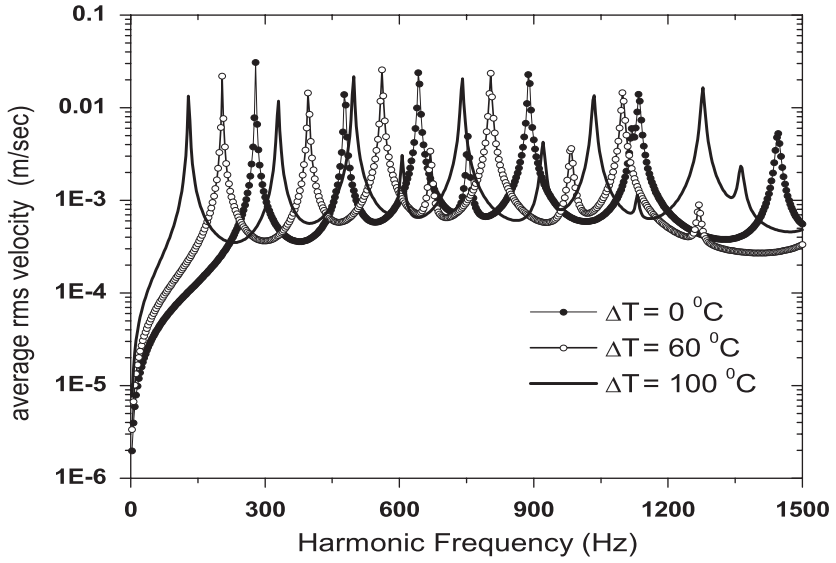

Fig. 6. Average *rms* velocity for a 45,° fiber orientation of a Glass/Epoxy composite plate.

with an increase in temperature. The trend of reduced resonant amplitudes cannot be clearly seen in higher modes of displacement. This, however, can be seen clearly in the velocity, average rms velocity and sound power-level responses. Generally, the pre-stress due to thermal load will reduce the stiffness of the structure which in turn increases the displacement amplitude of vibration. This is not seen in the response at resonant frequencies. This implies that the modal damping has a significant counterinfluence. Since the modal damping increases significantly with the temperature it reduces the vibration amplitude at the resonant frequencies. Similar responses are observed for other fiber orientations.

Fig. 7 shows the radiation efficiency for a 45° fiber orientation as a function of frequency. Sound power is directly proportional to the product of the square of the averaged surface normal velocity and radiation efficiency. Orthotropic plates have two coincidence frequencies: one corresponding to bending waves in the major direction (fiber direction) f_{cx} and another one corresponding to bending waves in the minor direction f_{cy}. The values of f_{cx} and f_{cy} were obtained from the analytical expression given by Ohlrich and Hugin [15].

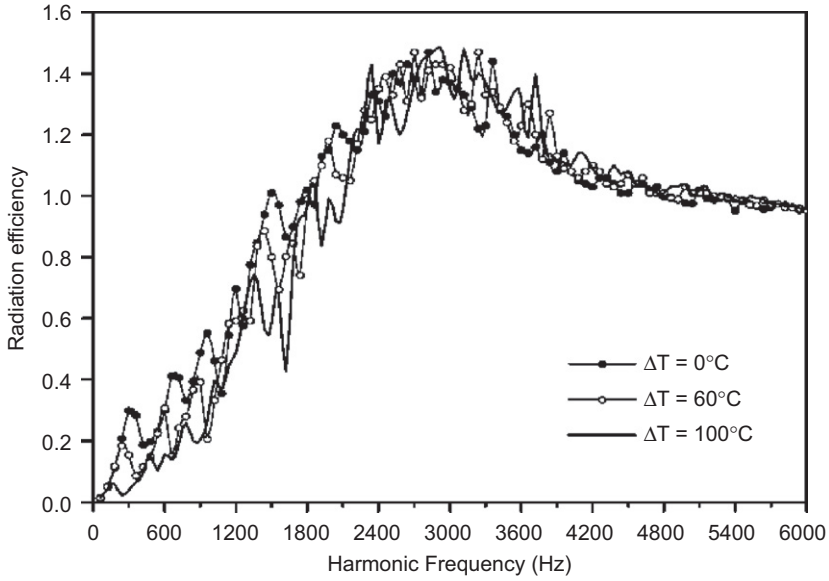

Fig. 7. Radiation efficiency for a 45° fiber orientation of a Glass/Epoxy composite plate.

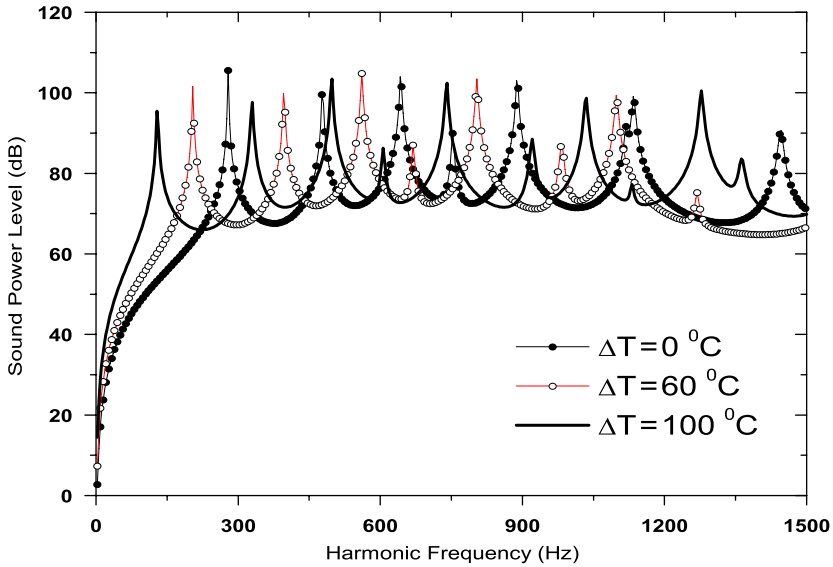

Fig. 8. Sound power level for a 45° fiber orientation of a Glass/Epoxy composite plate.

For the composite plate analyzed in the present work these frequencies are 1598 and 2564 Hz, respectively. Fig. 7 shows that radiation efficiency crosses one at the lower coincidence frequency and decreases towards one only after the second coincidence frequency.

From Fig. 7 it can be seen that the radiation efficiency of the plate generally decreases (no significant variation in the low-frequency range) with an increase in temperature. The sound power level shown in Fig. 8 reflects the average *rms* velocity response as sound radiation is directly related to the normal velocity of the structure at a particular frequency.For further investigation average of mean square velocity is calculated for the 45° fiber orientation in the entire frequency band as shown in Fig. 9 and for constant bandwidth frequency bands (250 Hz) as shown in Fig. 10. From Figs. 9 and 10 one can see that the velocity generally decreases with temperature. When the uniform temperature rise reaches 100 °C, which is closer to the critical buckling

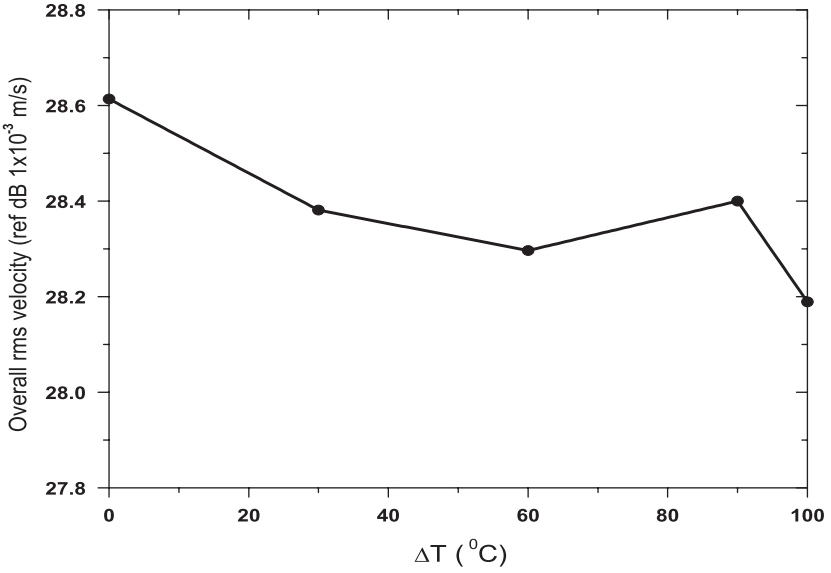

Fig. 9. Overall average *r*ms velocity for a 45° fiber orientation of a Glass/Epoxy composite plate.

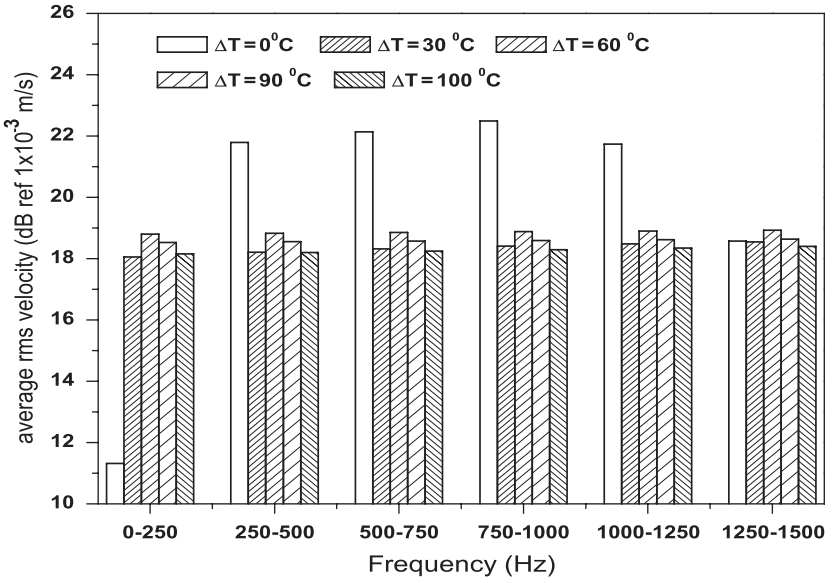

Fig. 10. Average *rms* velocity for a 45° fiber orientation of a Glass/Epoxy composite in constant frequency bands.

temperature for the different fiber orientations analyzed, there is a marginal reduction in the overall average rms velocity.

From the bandwise representation also it is clear that the rms velocity is higher when there is no rise in uniform temperature (except at the lower band) and is lower when the uniform temperature rise is 100 °C. This is due to a significant increase in the modal loss factor when the uniform temperature rise is closer to the critical buckling temperature of the structure. In the lower frequency band, the vibration response is influenced by the stiffness of the structure; it can be clearly seen in the displacement, velocity and average rms velocity responses.

To obtain a clearer picture, the overall sound power level for the entire frequency band is computed for different fiber orientations and the results are shown in Fig. 11. For all fiber orientations, it is clear that even though the overall sound power level is not significantly affected by the thermal environment, there is a

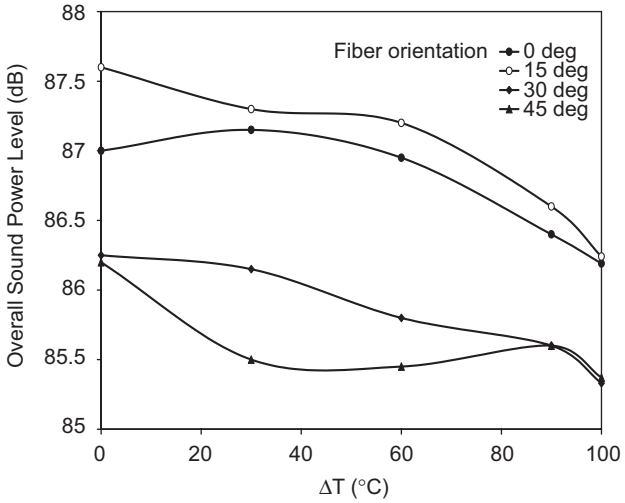

Fig. 11. Overall sound power level for different fiber orientations of a Glass/Epoxy composite plate.

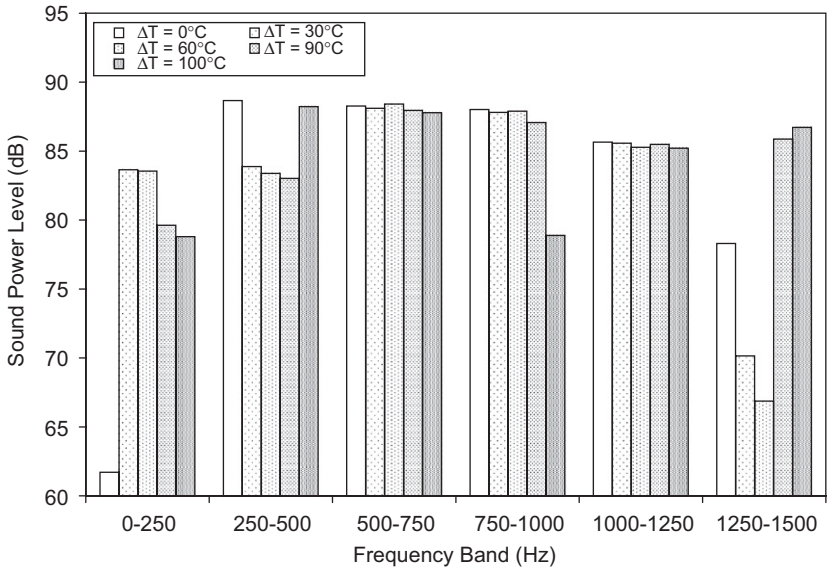

Fig. 12. Output power level for a 45° fiber orientation of a Glass/Epoxy composite in constant frequency bands.

distinct downward trend when the uniform temperature rise approaches the critical buckling temperature. Fig. 12 shows the sound power level represented in constant bandwidth frequency bands for the 45° fiber orientation. The shift in natural frequencies towards the lower bands due to an increase in uniform temperature rise will in turn reduce the normal velocity which is directly related to the sound power radiated. This can be seen in Fig. 12, where the sound power level decreases with an increase in uniform temperature rise beyond the initial increase from $\Delta T = 0$ to 30 °C.

The resonant amplitude of vibration response and acoustic response increases with temperature rise for an isotropic plate while the resonant amplitudes decrease with an increase in temperature rise for the composite plate with inherent material damping. Even though the structural stiffness reduces with an increase in temperature, the modal loss factor reduces the resonant amplitude as it increases significantly with temperature rise for the composite plate. Due to this reason, there is no significant change in the overall sound power level of the composite plate also. This would suggest that one could use a composite material having inherent material damping for structures subjected to a thermal field. Figs. 13 and 14 show the sound power

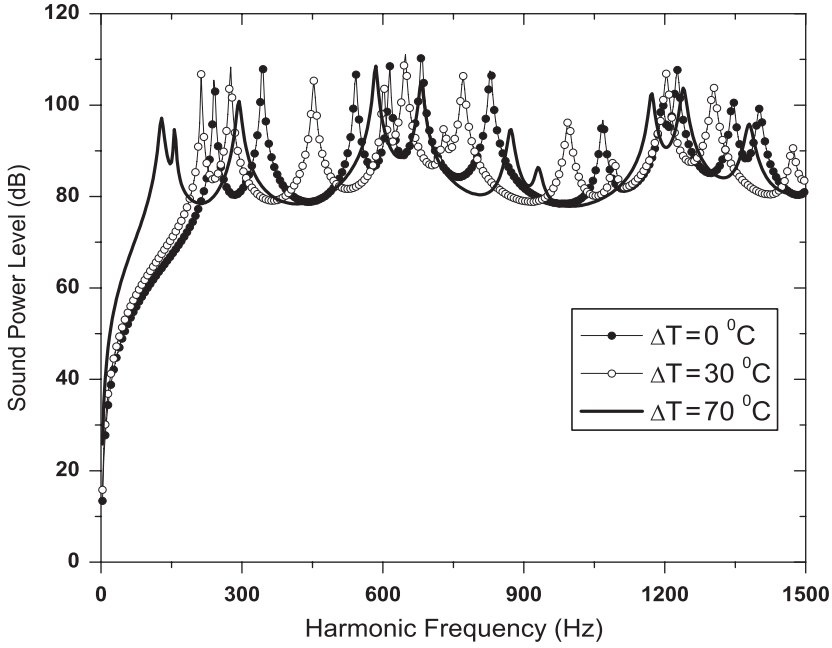

Fig. 13. Output power level for a PEEK/IM7 composite plate.

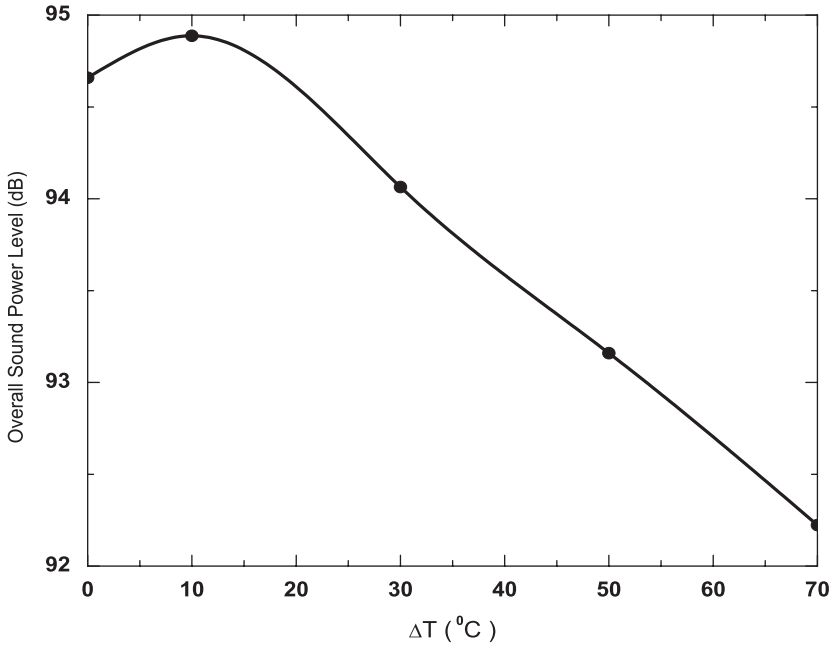

Fig. 14. Overall sound power level for a PEEK/IM7 composite plate.

response and overall sound power level of the PEEK/IM7 composite plate. From Fig. 13 one can see similar changes and acoustic responses can be seen for the PEEK/IM7 composite plate also. From Figs. 13 and 14 it is clear that there is no significant influence of temperature-dependent material properties on the vibration and acoustic response characteristics. This is again due to the competing effects of increased damping and reduced stiffness.

6. Conclusion

The effect of a thermal environment on the vibration response and consequent sound radiation from a composite plate for different values of fiber orientation is investigated. The calculations are performed for different fiber orientations and the clamped–clamped boundary conditions are assumed. Displacement and velocity at the point of excitation, average rms velocity, radiation efficiency and output sound power level are computed for different boundary conditions to show the influence of thermal loading on vibration response and sound radiation. It is found that the amplitudes of vibration at the resonant frequencies decrease with the increase in temperature. The resonant amplitude is less when the uniform temperature rise approaches the critical buckling temperature of the structure. From the studies carried out on PEEK/IM7, it is found that the influence of temperature-dependent material properties is not significant on the vibration and acoustic response of structures in a thermal environment. There is no significant change in the overall sound power level of a composite plate with material damping compared to an isotropic plate because of complementing effects of reduced stiffness and increased damping. The vibration and sound radiation of a composite plate is significantly influenced by inherent material damping when compared with an isotropic plate.

References

[1] R. Chandra, S.P. Singh, K. Gupta, Damping studies in fiber-reinforced composites a review, *Composite Structures* 46 (1999) 41–51.
[2] R. Rikards, Finite element analysis of vibration and damping of laminated composites, *Composite Structures* 24 (1993) 193–204.
[3] J.D.D. Melo, D.W. Radford, Time and temperature dependence of the viscoelastic properties of CFRP by dynamic mechanical analysis, *Composite Structures* 70 (2005) 240–253.
[4] N.N. Huang, T.R. Tauchert, Thermal buckling of clamped symmetric laminated plates, *Impact and Buckling of Structures, ASME Aerospace Division* 20 (1990) 53–59.
[5] H.R.H. Kabir, H. Askar, R.A. Chaudhuri, Thermal buckling response of shear flexible laminated anisotropic plates using a three-node isoparametric element, *Composite Structures* 59 (2003) 173–187.
[6] K.R. Thangaratnam, R. Palaninathan, J. Ramachandran, Thermal buckling of composite laminated plates, *Composite Structures* 32 (1989) 1117–1124.
[7] N. Ganesan, V. Pradeep, Buckling and vibration of rectangular composite viscoelastic sandwich plates under thermal loads, *Composite Structures* 77 (2007) 419–429.
[8] C.S. Lyrintzis, Hygrothermal effects on structure borne noise transmission of stiffened laminated composite plates, *Journal of Aircraft* 77 (1990) 722–730.
[9] J. Park, L. Mongeau, T. Siegmund, Influence of support properties on sound radiated from the vibrations of rectangular plates, *Journal of Sound and Vibration* 264 (2003) 775–794.
[10] Y. Qiao, Q. Huang, The effect of boundary conditions on sound loudness radiated from rectangular plates, *Archieve of Applied Mechanics* 264 (2007) 21–34.
[11] O.C. Zienkiewicz, *The Finite Element Method in Engineering Science*, McGraw-Hill Publishing Company Limited, London, 1971.
[12] Z. Tong, Y. Zhang, Z. Zhang, H. Hua, Dynamic behavior and sound transmission analysis of a fluid–structure coupled system using the direct-BEM/FEM, *Journal of Sound and Vibration* 299 (2007) 645–655.
[13] N. Alam, N.T. Asnanai, Vibration and damping analysis of fiber-reinforced composite material–plates, *Journal of Composite Materials* 20 (1986) 2–18.
[14] .S Li, X. Li, The effects of distributed masses on acoustic radiation behavior of plates, *Applied Acoustics* 69 (2008) 272–279.
[15] M. Ohlrich, C.T. Hugin, On the influence of boundary constraints and angle baffle arrangements on sound radiation from rectangular plates, *Journal of Sound and Vibration* 277 (2004) 405–418.